Coastal ocean acidification and increasing total alkalinity in the NW Mediterranean Sea

Lydia Kapsenberg[1], Samir Alliouane[1], Frédéric Gazeau[1], Laure Mousseau[1], and Jean-Pierre Gattuso[1,2,§]

[1]Sorbonne Universités, Université Pierre et Marie Curie-Paris 6, CNRS-INSU, Laboratoire d'Océanographie de Villefranche, 06230, Villefranche-sur-Mer, France

[2]Institute for Sustainable Development and International Relations, Sciences Po, 27 rue Saint Guillaume, F-75007 Paris, France

[§]Corresponding author

E-mail: gattuso@obs-vlfr.fr

Phone: +33 4 93 76 38 59

Abstract. Coastal time-series of ocean carbonate chemistry are critical for understanding how global anthropogenic change manifests in near-shore ecosystems. Yet, they are few and have low temporal resolution. At the time-series station Point B in the NW Mediterranean Sea, seawater was sampled weekly from 2007 through 2015, at 1 and 50 m, and analyzed for total dissolved inorganic carbon (C_T) and total alkalinity (A_T). Parameters of the carbonate system such as pH (pH_T, total hydrogen ion scale) were calculated and a deconvolution analysis was performed to identify drivers of change. The rate of surface ocean acidification was -0.0028 ± 0.0003 units pH_T yr^{-1}. This rate is larger than previously identified open-ocean trends due rapid warming that occurred over the study period (0.072 ± 0.022 °C yr^{-1}). The total pH_T change over the study period was of similar magnitude as the diel pH_T variability at this site. The acidification trend can be attributed to atmospheric carbon dioxide (CO_2) forcing (59 %, 2.08 ± 0.01 ppm CO_2 yr^{-1}) and warming (41 %). Similar trends were observed at 50 m but rates were generally slower. At 1 m depth, the increase in atmospheric CO_2 accounted for approximately 40 % of the observed increase in C_T (2.97 ± 0.20 μmol kg^{-1} yr^{-1}). The remaining increase in C_T may have been driven by the same unidentified process that caused an increase in A_T (2.08 ± 0.19 μmol kg^{-1} yr^{-1}). Based on the analysis of monthly trends, synchronous increases in C_T and A_T were fastest in the spring-summer transition. The driving process of the interannual increase in A_T has a seasonal and shallow component, which may indicate riverine or groundwater influence. This study exemplifies the importance of understanding changes in coastal carbonate chemistry through the lens of biogeochemical cycling at the land-sea interface. This is the first coastal acidification time-series providing multiyear data at high temporal resolution. The data confirm rapid warming in the Mediterranean Sea and demonstrate coastal acidification with a synchronous increase in total alkalinity.

Keywords – ocean change, ocean acidification, time-series, pH, alkalinity, dissolved inorganic carbon, pCO_2, Mediterranean Sea

1. Introduction

Maintaining time-series of oceanographic data is essential for understanding anthropogenic changes in the ocean (Tanhua et al., 2013). On land, fossil fuel burning, cement production, and land use changes have contributed ~600 Gt carbon to the atmosphere during the period 1750-2015 (Le Quéré et al., 2016). In the recent decade 2006-2015, an estimated 25 % of this anthropogenic carbon has been absorbed by the ocean in the form of carbon dioxide (CO_2; Le Quéré et al., 2016), and is causing global changes to the ocean carbonate system. Absorption of CO_2 by seawater produces carbonic acid, which decreases seawater pH, and is of great concern for biological processes and marine ecosystems (Doney et al., 2009; Gattuso and Hansson, 2011; Pörtner et al., 2014). Since the preindustrial era, global mean ocean pH has declined by 0.1 (Rhein et al., 2013). Due to the declining trend of ocean pH with increasing anthropogenic CO_2, the process is termed 'ocean acidification'. This expression represents a suite of chemical changes, including increases in total dissolved inorganic carbon (C_T) and partial pressure of CO_2 (pCO_2) and decrease in calcium carbonate saturation states (Ω, aragonite and calcite; Dickson, 2010). Rates of ocean acidification differ by ocean region and range from -0.0026 (Irminger Sea, North Atlantic) to -0.0013 (South Pacific) units pH yr^{-1} (Bates et al., 2014). Such time-series remain spatially limited, especially in coastal regions, which provide valuable ecosystem services (Barbier et al., 2011; Costanza et al., 1997) and are under high anthropogenic impact (Halpern et al., 2008). Here, we present the first coastal ocean acidification time-series at high temporal resolution.

Compared to the global ocean, marginal seas serve a critical role in anthropogenic CO_2 storage via enhanced CO_2 uptake and export to the ocean interior (Lee et al., 2011). As a marginal sea, the Mediterranean Sea has a naturally high capacity to absorb but also buffer anthropogenic CO_2 (Álvarez et al., 2014; Palmiéri et al., 2015). This is primarily due to the high total alkalinity (A_T) of Mediterranean waters and overturning circulation (Lee et al.,

66 2011; Palmiéri et al., 2015; Schneider et al., 2010). In the Mediterranean Sea, the salinity-A_T
67 relationship is driven by the addition of river discharge and Black Sea input, which are
68 generally high in A_T (Copin-Montégut, 1993; Schneider et al., 2007). Combined with
69 evaporation, this results in higher A_T and salinity in the Mediterranean Sea compared to the
70 Atlantic Mediterranean source water (Jiang et al., 2014). On average, Mediterranean Sea A_T
71 is 10 % higher than in the global ocean (Palmiéri et al., 2015). The surface ocean
72 acidification rate, estimated at ΔpH_T (total hydrogen ion scale) of -0.08 since 1800, is
73 comparable to that of the global ocean despite a 10 % greater anthropogenic carbon inventory
74 (Palmiéri et al., 2015). Due to its important role in carbon sequestration and ecological
75 sensitivity to anthropogenic change with economic consequences (Lacoue-Labarthe et al.,
76 2016), the Mediterranean Sea could provide insight to global trends (Lejeusne et al., 2010).
77 Over the last few years, numerous studies have estimated ocean acidification rates
78 across the Mediterranean Sea (Table 1). Together, these studies cover various periods with a
79 range of techniques yielding different results. For example, estimates of change in pH of
80 bottom waters since the preindustrial era range between -0.005 to -0.06 (Palmiéri et al., 2015)
81 and as much as -0.14 for full profile estimates (Touratier and Goyet, 2011). Techniques for
82 estimating ocean acidification in the Mediterranean Sea thus far include: (1) hind-casting,
83 using high-resolution regional circulation models (Palmiéri et al., 2015), the TrOCA
84 approach as applied to cruise-based profile data (Krasakopoulou et al., 2011; Touratier and
85 Goyet, 2011; Touratier et al., 2016) and others (Howes et al., 2015), (2) partially
86 reconstructed time-series (Marcellin Yao et al., 2016), (3) comparative study periods
87 (Luchetta et al., 2010; Meier et al., 2014), and (4) sensor-based observations over a short
88 study period (Flecha et al., 2015). Ocean acidification time-series of consistent sampling over
89 many years are lacking for the Mediterranean Sea (The MerMex Group et al., 2011),

90 particularly along the coast where river discharge influences the carbonate system (Ingrosso
91 et al., 2016).
92 Compared to the open ocean, shallow coastal sites exhibit natural variability in
93 carbonate chemistry over annual timeframes (Hofmann et al., 2011; Kapsenberg and
94 Hofmann, 2016; Kapsenberg et al., 2015), complicating the detection and relevance of open
95 ocean acidification in isolation of other processes (Duarte et al., 2013). In the NW Pacific
96 coast, rapid acidification of surface waters (ΔpH_T -0.058 units yr^{-1}) at Tatoosh Island was
97 documented in the absence of changes in known drivers of local pH variability (e.g.,
98 upwelling, eutrophication, and more; Wootton and Pfister, 2012; Wootton et al., 2008).
99 Further inshore, in the Hood Canal sub-basin of the Puget Sound, only 24-49 % of the
100 estimated pH decline from pre-industrial values could be attributed to anthropogenic CO_2
101 (Feely et al., 2010). The excess decrease in pH was attributed to increased remineralization
102 (Feely et al., 2010). Acidification rates documented along the North Sea Dutch coastline and
103 inlets were highly variable in space, with some exceeding the expected anthropogenic CO_2
104 rate by an order of magnitude while others exhibited an increase in pH (Provoost et al.,
105 2010).
106 Variability in coastal carbonate chemistry stems from both physical (e.g., upwelling,
107 river discharge; Feely et al., 2008; Vargas et al., 2016) and biological processes (e.g., primary
108 production, respiration, net calcification). Within watersheds, coastal carbonate chemistry is
109 affected by eutrophication (Borges and Gypens, 2010; Cai et al., 2011), groundwater supply
110 (Cai et al., 2003), and land use and rain influence on river alkalinity (Raymond and Cole,
111 2003; Stets et al., 2014). Over longer periods, pH can also be influenced by atmospheric
112 deposition (Omstedt et al., 2015). Through primary production and respiration, coastal
113 ecosystems produce pH fluctuations over hours (e.g., seagrass, kelp) to months (e.g.,
114 phytoplankton blooms; Kapsenberg and Hofmann, 2016). Due to existing pH variability in

coastal seas, it is necessary to quantify high-frequency trends in order to interpret the pH changes inferred from lower-frequency sampling.

In this study, we present the first complete time-series data quantifying the present-day ocean acidification rate for a coastal site in the Mediterranean Sea, based on weekly measurements of A_T and C_T sampled from 2007 through 2015. For a subset of this time-series, pH variability was documented using a SeaFET™ Ocean pH Sensor in order to assess hourly pH variability. For comparison and consistency with other ocean acidification time-series around the world, we report rates of change based on anomalies (Bates et al., 2014) and identify drivers of change.

2. Materials and methods

2.1. Site description

A carbonate chemistry time-series was initiated in 2007 and maintained through 2015 in the NW Mediterranean Sea at the entrance of the Bay of Villefranche-sur-Mer, France (Fig. 1): Point B station (43.686° N, 7.316° E, 85 m bottom depth). A second site, Environment Observable Littoral buoy (EOL, 43.682° N, 7.319° E, 80 m bottom depth), was used for pH sensor deployment starting in 2014. These two sites are 435 m apart. Point B has been an oceanographic station since 1957. A full site description and research history has been detailed by De Carlo et al. (2013). Briefly, the Bay is a narrow north-south facing inlet with steep bathymetry and estimated volume of 310 million m^3. The surrounding region is predominantly composed of limestone with a series of shallow, submarine groundwater karst springs (Gilli, 1995). The North current, a major and structuring counter-clockwise current in the Ligurian Sea, can sometimes flow close to Point B. The Bay can also be, on occasion, influenced by local countercurrents. Both of these hydrodynamics movements have

signatures of river discharge. Limestone erosion can be observed in the A_T of rivers nearest to Point B (Paillon, due 4 km West; Var due 10 km West; and Roya due 26 km East). River A_T ranges between 1000 to 2000 μmol kg^{-1} (data from *Agence de l'Eau Rhône-Méditerranée-Corse*, http://sierm.eaurmc.fr), and is lower than seawater A_T. The Paillon River, whose plume on occasion reaches into the Bay (L. Mousseau, pers. obs.), was sampled on 18 August 2014 and had a A_T of 1585 ± 0.1 μmol kg^{-1} (N = 2, J.-P. Gattuso, unpubl.). Due to low primary productivity, seasonal warming drives the main annual variability in carbonate chemistry at this location (De Carlo et al., 2013).

2.2. Point B data collection, processing, and analysis

To document long-term changes in ocean carbonate chemistry at Point B, seawater was sampled weekly from 9 January 2007 to 22 December 2015. Samples were collected at 1 and 50 m, using a 12-L Niskin bottle at 9:00 local time. Seawater was transferred from the Niskin bottle to 500 mL borosilicate glass bottles and fixed within an hour via addition of saturated mercuric chloride for preservation of carbonate parameters, following recommendations by Dickson et al. (2007). Duplicate samples were collected for each depth. For each sampling event, CTD casts were performed either with a Seabird 25 or Seabird 25+ profiler whose sensors are calibrated at least every two years. Accuracy of conductivity (SBE4 sensor) and temperature (SBE3 sensor) measurements from CTD casts were 0.0003 S m^{-1} and 0.001°C, respectively.

Within six months of collection, bottle samples were analyzed for C_T and A_T via potentiometric titration following methods described by Edmond (1970) and DOE (1994), by *Service National d'Analyse des Paramètres Océaniques du CO_2*, at the Université Pierre et Marie Curie in Paris, France. Average accuracy of C_T and A_T measurements was 2.6 and 3 μmol kg^{-1}, respectively, as compared with seawater certified reference material (CRM)

provided by A. Dickson (Scripps Institution of Oceanography). Repeatability of replicate samples was better than 3 µmol kg^{-1}. Only obvious outliers were omitted from the analyses: three C_T values at 1 m (> 2300 µmol kg^{-1}), one A_T value at 1 m (> 2900 µmol kg^{-1}), and one A_T value at 50 m (< 2500 µmol kg^{-1}). The C_T and A_T measurements on replicate bottle samples were averaged for analyses.

Calculations of the carbonate system parameters were performed using the R package seacarb version 3.1 with C_T, A_T, *in situ* temperature, and salinity as inputs (Gattuso et al., 2016). Total concentrations of silicate ($SiOH_4$) and phosphate (PO_4^{3-}) were used when available from Point B (L. Mousseau, unpubl., http://somlit.epoc.u-bordeaux1.fr/fr/). Detection limits for nutrients were 0.03 µM for $SiOH_4$ and 0.003 to 0.02 µM for PO_4^{3-}; relative precision of these analyses is 5-10 % (Aminot and Kérouel, 2007). Total boron concentration was calculated from salinity using the global ratio determined by Lee et al. (2010). The following constants were used: K_1 and K_2 from Lueker et al. (2000), K_f from Perez and Fraga (1987), and K_s from Dickson (1990). Reported measured parameters are temperature, salinity, A_T, and C_T, and derived parameters are pH_T (total hydrogen ion scale), pH_T normalized to 25 ºC (pH_{T25}), pCO_2, and aragonite (Ω_a) and calcite (Ω_c) saturation states. Salinity-normalized changes in A_T (nA_T) and C_T (nC_T) were calculated by dividing by *in situ* salinity and multiplying by 38. Except for pH_{T25}, all parameters are reported at *in situ* temperatures.

The average uncertainties of the derived carbonate parameters were calculated according to the Gaussian method (Dickson and Riley, 1978) implemented in the "errors" function of the R package seacarb 3.1 (Gattuso et al., 2016). The uncertainties are ± 2.7 x 10^{-10} mol H^+ (about 0.015 units pH_T), ± 15 µatm pCO_2, and ± 0.1 unit of the aragonite and calcite saturation states.

To quantify interannual changes in carbonate parameters, the data were detrended for seasonality by subtracting the respective climatological monthly means computed for the period 2009-2015 from the time-series ('monthly means' from hereon). The resulting residuals were analyzed using a linear regression to compute anomaly trends. This approach follows methods from Bates et al. (2014) to allow for comparisons of trends observed at different time-series stations. All analyses were performed in R (R Core Team, 2016).

2.3. Deconvolution of pH_T and pCO_2

To identify proportional contributions of various drivers to ocean acidification trends at Point B, deconvolution of time-series pH_T and pCO_2 was performed following methods from García-Ibáñez et al. (2016) for observations at 1 and 50 m. The equation is described below for pH_T, where changes in pH_T are driven by changes in temperature (T), salinity (S), A_T, and C_T, over time (t):

$$\frac{dpH_T}{dt} = \frac{\partial pH_T}{\partial T}\frac{dT}{dt} + \frac{\partial pH_T}{\partial S}\frac{dS}{dt} + \frac{\partial pH_T}{\partial A_T}\frac{dA_T}{dt} + \frac{\partial pH_T}{\partial C_T}\frac{dC_T}{dt} \quad (1)$$

Here, $\frac{\partial pH_T}{\partial var}\frac{dvar}{dt}$ represents the slope contribution of changing *var* to the estimated change in pH_T ($\frac{dpH_T}{dt}$), where *var* is either temperature (T), salinity (S), A_T, or C_T. The sensitivity of pH to *var* ($\frac{\partial pH_T}{\partial var}$) was estimated by calculating pH_T using the true observations of *var* and holding the other three variables constant (mean value of the time-series) and regressing it to *var*. Sensitivity ($\frac{\partial pH_T}{\partial var}$) was then multiplied by the anomaly rate of *var* (Table 2). The calculation was repeated for pCO_2 ($\frac{dpCO_2}{dt}$) in order to compare the rate of increase with that of atmospheric CO_2.

As a sub-component of $\frac{\partial pCO_2}{\partial C_T}\frac{dC_T}{dt}$, the rate of anthropogenic CO_2 increase was estimated from atmospheric CO_2 concentrations nearest to Point B (Plateau Rosa, Italy,

courtesy of the World Data Center for Greenhouse Gases, http://ds.data.jma.go.jp/gmd/wdcgg/). For these data, missing daily values were linearly interpolated, climatological monthly means were calculated and subtracted from the time-series to generate an anomaly time-series. A linear regression was performed on anomalies where the slope represents the rate of anthropogenic CO_2 increase in the atmosphere. Finally, to help identify different processes that might have contributed to the observed trends, linear regressions were performed on changes in A_T and C_T per month (mean value of observations within one month) from 2009 through 2015 and on the salinity-A_T relationship by year.

2.4. SeaFET data collection, processing, and analysis

To capture pH variability at higher-than-weekly sampling frequencies, a SeaFET™ Ocean pH sensor (Satlantic) was deployed on the EOL buoy (435 m from the Point B sampling site) starting in June 2014, at 2 m depth. Autonomous sampling was hourly and deployment periods averaged 58 ± 25 days with 5 ± 2 calibration samples per deployment.

Field calibration samples for pH were collected using a Niskin bottle next to SeaFET within 15 min of measurement. This sampling scheme was sufficient for this site as there is no large high-frequency pH variability. Unlike Point B sampling, SeaFET calibration samples were processed for pH using the spectrophotometric method (Dickson et al., 2007) with purified m-cresol purple (purchased from the Byrne lab, University of South Florida). *In situ* temperature, salinity, and A_T measured at Point B, within 30 min of the SeaFET sampling, were used to calculate *in situ* pH_T of the calibration samples.

SeaFET voltage was converted to pH_T using the respective calibration samples for each deployment period, following the methods and code described in Bresnahan et al. (2014) but adapted for use in R. Only 5 % of the data was removed during quality control, due to biofouling in one deployment and battery exhaustion in another, yielding 610 days of

data. The mean offset between calibration samples and the calibrated SeaFET pH time-series was ± 0.007, indicating a high-quality pH dataset (data shown in Fig. 7c).

The estimated standard uncertainty in SeaFET pH_T is ± 0.01 and was calculated as the square root of the sum of each error squared. The sources of errors are: measurement error of spectrophotometric pH (± 0.004, N = 68 mean SD of 5 replicate measurements per calibration sample for samples collected between 16 July 2014 and 3 May 2016), spatio-temporal mismatch sampling at EOL (± 0.007, mean offset of pH_T of the calibration samples from calibrated time-series), and variability in purified m-cresol dye batch accuracy as compared to Tris buffer CRM pH (± 0.006, mean offset of pH_T of the spectrophotometric measurement of Tris buffer from the CRM value).

3. Results

3.1. Time-series trends

At Point B from January 2007 to December 2015, more than 400 samples were collected for carbonate chemistry at both 1 and 50 m. Anomaly trends detected at 1 m (Fig. 2) were also significant at 50 m (Fig. 3, Table 2), with the exception that salinity only increased at 50 m (0.0063 ± 0.0020 units yr^{-1}). At 1 m, trends were significant for pH_T (-0.0028 units yr^{-1}), A_T (2.08 µmol kg^{-1} yr^{-1}), C_T (2.97 µmol kg^{-1} yr^{-1}), pCO_2 (3.53 µatm yr^{-1}), and Ω_a (-0.0064 units yr^{-1}). At the same time, temperature anomaly increased (0.072 ºC yr^{-1}). Changes in carbonate chemistry parameters were greater at 1 m compared to 50 m, with the exception of salinity and temperature. The warming rate at 50 m was slightly greater compared to 1 m, mostly due to increasing summer temperatures since 2007.

Strong seasonal cycles of carbonate chemistry parameters were present at Point B at 1 m (Fig. 4). Climatological monthly means (2007-2015) are described briefly and listed in

Table S1. Mean temperature range was 11.2 ºC with a maximum at 24.77 ± 1.35 ºC in August and minimum of 13.58 ± 0.41 ºC in February. The range in A_T was 19 µmol kg^{-1} from June to September. The C_T range was 33 µmol kg^{-1} with a peak in late winter and minimum values in August and October. Due to summer warming coinciding with the period of peak primary productivity (De Carlo et al. 2013), warming countered the influence of low C_T on pH. As a result, pH_T reached minimum values in summer (8.02 ± 0.03, July and August) and peaked in late winter (8.14 ± 0.01, February and March), for an overall annual pH range of 0.12. The corresponding pCO_2 range was 128 µatm from February to August. Seasonal cycles were smaller at 50 m compared to 1 m (Table S1).

3.2. Deconvolution of pH_T and pCO_2

Deconvolutions of pH and pCO_2 are presented in Table 3 and 4, respectively. The estimated anomaly trends ($\frac{dpH_T}{dt}$,$\frac{dpCO_2}{dt}$) from the deconvolution fall within the error of the observed anomaly trends (Table 2). The contribution of warming to the pH_T anomaly (-0.0011 units yr^{-1}, at 1 m) matched the difference between the trends of pH_T and pH_{T25C} (Table 2), which verifies that the deconvolution reproduced influences of temperature sensitivity well. Overall, these results indicate that the deconvolution analyses represent the observed trends well.

At both depths, the predominant driver of $\frac{dpH_T}{dt}$ and $\frac{dpCO_2}{dt}$ was the increase in C_T. Increasing A_T countered 66-69 and 60 % of the influence of increasing C_T on $\frac{dpH_T}{dt}$ and $\frac{dpCO_2}{dt}$, respectively. At 1 m, warming accounted for 41 and 37 % of $\frac{dpH_T}{dt}$ and $\frac{dpCO_2}{dt}$, respectively. Since warming was slightly greater at 50 m compared to 1 m, warming accounted for a larger proportional influence on $\frac{dpH_T}{dt}$ and $\frac{dpCO_2}{dt}$ at 50 m compared to 1 m. Increasing salinity at 50 m contributed slightly to $\frac{dpH_T}{dt}$ (4 %) and $\frac{dpCO_2}{dt}$ (2 %).

286 Atmospheric CO_2 anomaly at Plateau Rosa increased by 2.08 ± 0.01 ppm yr^{-1} ($F_{1,3285}$
287 = 4664, P <<0.001, R^2 0.93) during the study period 2007-2015, and represents the
288 anthropogenic CO_2 forcing on seawater pH. To estimate the influence of anthropogenic CO_2
289 forcing at Point B, we assume air-sea CO_2 equilibrium (e.g., increase in atmospheric CO_2
290 causes an equal increase in seawater pCO_2) for the water mass at 1 m. This assumption is
291 based on evidence that Point B is a weak sink for atmospheric CO_2 with near-balanced air-sea
292 CO_2 flux on an annual time-frame (De Carlo et al., 2013). Considering the error associated
293 with deconvolution of pCO_2 at 1 m, atmospheric CO_2 increase can, at most, represent 38-43
294 % of the total C_T contribution ($\frac{\partial pCO_2}{\partial C_T}\frac{dC_T}{dt}$) to $\frac{dpCO_2}{dt}$. This leaves 57-62 % of the total C_T
295 contribution to pCO_2 trends unaccounted for.
296 As A_T is not influenced by addition of anthropogenic CO_2 to seawater, but it did
297 increase, the next question was whether or not the changes in A_T and C_T were process-linked.
298 At 1 m, regressions of annual monthly trends of A_T and C_T revealed similar seasonal cycles
299 for both parameters (Fig. 5, Table S2). The fastest increases in A_T and C_T occurred from May
300 through July. The smallest (non-significant) changes occurred in January. The synchronicity
301 between monthly trends of A_T and C_T was also observed at 50 m, but the rates were slower
302 (analysis not shown).
303
304 **3.3. Salinity and A_T relationships**
305 Over an annual observation period at 1 m, salinity was a poor predictor of A_T, with the
306 exception of 2007 (Fig. 6). The R^2 value for each annual salinity-A_T relationship at 1 m
307 ranged from 0.00 (in 2013) to 0.87 (in 2007) with y-intercepts (A_{T0}, total alkalinity of the
308 freshwater end-member) ranging between -176 µmol kg^{-1} (in 2007) and 2586 µmol kg^{-1} (in
309 2013). The interannual variability of the salinity-A_T relationship was driven by the variability
310 in A_T observed at salinity < 38.0 that was present from November through July.

311 Changes in salinity (based on monthly means) at Point B were small and ranged from
312 37.64 ± 0.26 to 38.21 ± 0.11 from May to September, following freshwater input in winter
313 and spring and evaporation throughout summer and fall (Fig. 4). Highest (> 38.0) and most
314 stable salinity observations were made in August through October and coincided with the
315 period of maximum A_T (2562 and 2561 ± 9 µmol kg^{-1} in September and October,
316 respectively). Minimum A_T (2543 ± 14 µmol kg^{-1}) was observed in June, one month after
317 minimum salinity. To capture this seasonality without the inter-annual variation of A_T, the
318 salinity-A_T relationship at 1 m was estimated from climatological monthly means (cA_T and
319 *cS, N=12*) where cA_T units are µmol kg^{-1} and error terms are standard errors (R^2 = 0.74):

320 $$cA_T = 1554.9(\pm 185.9) + 26.3(\pm 4.9) \times cS \qquad (2)$$

321 At 50 m, monthly salinity and A_T were less correlated over an annual cycle (analysis not
322 shown). Salinity remained stable at 38.0 from January through September while A_T declined
323 by 13 µmol kg^{-1}. In general, seasonal changes were dampened at 50 m compared to 1 m.
324
325 **3.4. High-frequency pH data**
326 To verify the weekly sampling scheme at Point B, a continuous record of high-
327 frequency pH observations was obtained via SeaFET deployments from June 2014 to April
328 2016 (Fig. 7). Sensor data corroborated the seasonal pH and temperature cycle observed at
329 Point B (Fig. 7a-b). Event-scale effects (e.g., pH_T change ≥ 0.1 for days to weeks, *sensu*
330 Kapsenberg and Hofmann 2016) were absent at this site suggesting that weekly sampling was
331 sufficient to describe seasonal and interannual changes in carbonate chemistry at Point B.
332 The magnitude of diel pH_T variability was small: the 2.5th to 97.5th percentiles ranged
333 between 0.01 and 0.05 units pH_T (Fig. 7d-e). Variability increased from winter to spring with
334 the greatest variations in April, May, and June (ΔpH_T >0.035). The magnitude of diel pH

335 variability was not correlated with temperature or the concentration of chlorophyll-a (data not
336 shown).
337
338 **4. Discussion**
339 High resolution time-series are necessary to document coastal ocean acidification.
340 Based on weekly measurements from 2007 through 2015, near-surface pH_T decreased by
341 0.0028 ± 0.0003 units yr^{-1} at Point B in the NW coastal Mediterranean Sea. Temperature
342 increased by 0.072 ± 0.022 °C yr^{-1}. In addition, A_T increased by 2.08 ± 0.19 μmol kg^{-1} yr^{-1}, a
343 change that is unrelated to direct effects of CO_2 absorption by seawater. In less than a decade,
344 the total change in pH at Point B (ΔpH_T: 0.0252, Table 1) was of the same magnitude as the
345 diel pH variability (ΔpH_T: 0.01-0.05) and $1/5^{th}$ of the magnitude of the seasonal pH cycle
346 (ΔpH_T: 0.12) found at this site.
347 We can identify the drivers of ocean acidification at Point B using the deconvolution
348 of pH and pCO_2 trends and by assuming that the increase in A_T was due to increases in its
349 carbon constituents, bicarbonate (HCO_3^-) and carbonate (CO_3^{2-}) ions. This assumption is
350 based on the fact that (1) HCO_3^- and CO_3^{2-} ions together make up 96 % of A_T at Point B, (2)
351 increases in HCO_3^- and CO_3^{2-} would both contribute to A_T and C_T and thereby explain the
352 observed synchronicity of monthly trends in A_T and C_T (Fig. 5). Using the pCO_2
353 deconvolution, we can then sum the contributions to pCO_2 from A_T (-3.08 μatm pCO_2 yr^{-1})
354 and C_T (5.14 μatm pCO_2 yr^{-1}) to determine the proportional contribution of ΔC_T to ΔpCO_2
355 that is unrelated to changes in C_T brought on by A_T. This remaining 2.06 μatm pCO_2 yr^{-1}
356 increase due to increasing C_T closely matched the magnitude of atmospheric CO_2 increase
357 during the observation period (2.08 ± 0.01 ppm yr^{-1} at Plateau Rosa, Italy). The closeness of
358 these numbers does not imply causation. However, given that surface waters at Point B
359 exhibit a near-zero air-sea CO_2 flux over annual cycles (De Carlo et al., 2013), the evidence

360 supports the conclusion that the ocean acidification trend at Point B closely follows the rate
361 of atmospheric CO_2 increase. The influence of atmospheric CO_2 can also be observed in the
362 monthly changes in C_T. Monthly C_T trends are positive and statistically significant over more
363 months than A_T trends (8 vs. 3 months), which are more seasonally restricted (Fig. 5).
364 Applying this simple model to pH_T, assuming changes in C_T are due to both
365 increasing A_T (a neutralizing effect) and atmospheric CO_2 forcing, the surface ocean
366 acidification trend at Point B can be attributed primarily to atmospheric CO_2 forcing (59 %)
367 and secondarily to warming (41 %).
368 Using this same approach for observations at 50 m, the C_T contribution to pCO_2
369 trends that was unrelated to A_T change was 1.41 μatm pCO_2 yr^{-1}, which is 68 % of the rate of
370 atmospheric CO_2 increase in contrast to 99 % at 1 m. Changes in pH_T can then be attributed
371 to atmospheric CO_2 forcing (42 %), warming (54 %), and increasing salinity (3 %). Due to
372 slightly enhanced warming and reduced CO_2 penetration observed at 50 m, warming had a
373 greater effect on the ocean acidification trend than atmospheric CO_2 forcing at depth
374 compared to the surface.
375 The acidification rate at Point B (-0.0028 units pH_T yr^{-1}) is larger than those reported
376 for other ocean time-series sites (-0.0026 to -0.0013 units pH yr^{-1}, Bates et al., 2014), likely
377 due to differences in warming rates. The observed warming from 2007 through 2015 (0.72 to
378 0.88 ± 0.2 °C $decade^{-1}$) is extremely rapid relative to global trends in the upper 75 m from
379 1971 to 2010 (0.11 °C $decade^{-1}$, Rhein et al., 2013). The coastal region of Point B has
380 warmed steadily since 1980 and with periods of rapid warming (Parravicini et al., 2015).
381 Exacerbated warming may be related to the positive phases of the Atlantic Multi-decadal
382 Oscillation (AMO) and North Atlantic Oscillation (NAO), both of which are associated with
383 episodic warming of the Mediterranean Sea (Lejeusne et al., 2010). The AMO has been

384 positive since the 1990s[1] and positive NAO phases were prevalent during the second half of
385 our study[2].

386 Nearest to Point B, the acidification rate at DYFAMED, an open-sea site about 50 km
387 offshore from Point B (Fig. 1), was estimated at -0.003 ± 0.001 units pH_{SW} yr^{-1} from 1995 to
388 2011 (Marcellin Yao et al., 2016). At DYFAMED, warming contributed approximately 30 %
389 to the acidification rate and the remaining 70 % was attributed to anthropogenic CO_2
390 (Marcellin Yao et al., 2016). While the uncertainty for DYFAMED pH data is large, the
391 trends are comparable to those observed at Point B. However, A_T at the DYFAMED did not
392 change significantly from 2007 through 2014 ($F_{1,51}$ 3.204, P = 0.0794, R^2 0.08, data from
393 Coppola et al., 2016). This probably indicates that the processes driving changes in A_T at
394 Point B are unique to the coastal environment.

395 Similar changes in coastal carbonate chemistry were observed elsewhere in the near-
396 shore Mediterranean Sea. In the Northern Adriatic Sea, Luchetta et al. (2010) determined an
397 acidification rate of -0.0025 units pH_T yr^{-1} and an increase in A_T of 2.98 μmol kg^{-1} yr^{-1} at
398 depths shallower than 75 m, by comparing cruise data between the winters of 1983 and 2008.
399 Point B and Adriatic Sea observations are independent but reflect changes in seawater
400 chemistry that may be occurring in more coastal regions of the Mediterranean. Additional
401 time-series would help resolve the spatial extent of these observations.

402 While the trends in atmospheric CO_2 forcing and temperature account for the ocean
403 acidification trend at Point B, the increase in A_T and C_T beyond what can be attributed to
404 changes in atmospheric CO_2 was unexpected. The fastest increases in A_T and C_T occurred
405 from May through July (Fig. 5), when the thermal stratification settles. In the NW
406 Mediterranean, the main processes governing seasonal variability in A_T are evaporation

[1] http://www.cgd.ucar.edu/cas/catalog/climind/AMO.html
[2] http://www.cpc.ncep.noaa.gov/products/precip/CWlink/pna/month_nao_index.shtml

increasing A_T in summer (i.e., June through September at Point B) and, to a lesser extent, phytoplankton uptake of nitrate (NO_3^-) and phosphate (PO_4^{3-}) increasing A_T from January through March (Cossarini et al., 2015). During the transition of these processes, salinity decreases to a minimum in May, reflecting freshwater input that dilutes A_T to minimum values at the start of summer. For C_T, peak values occur in winter when the water column is fully mixed. For reference, at DYFAMED, mixing occurs down to more than 2000 m depth and C_T is up to 100 μmol kg^{-1} higher in deep waters (Copin-Montégut and Bégovic, 2002). Notably, monthly trends of C_T at Point B were not statistically significant from November through January for the period 2007-2015. Following winter, C_T declines due to a combination of phytoplankton bloom carbon uptake and freshwater dilution (assuming river C_T < seawater C_T), until the onset of summer stratification. Summer warming leads to pCO_2 outgassing (De Carlo et al., 2013), thereby further decreasing C_T. In addition, the increases in A_T and C_T from 2007 through 2015 were more pronounced at 1 m compared to 50 m. Thus, the process driving A_T and C_T trends are stronger at the surface and affect carbonate chemistry primarily during the spring-summer transition from May through July.

Identifying the process causing an increase in A_T and C_T beyond what can be attributed to changes in atmospheric CO_2 requires some speculation. Some biogeochemical processes can be ruled out as drivers. For example, changes in benthic processes are very unlikely. Reduced calcium carbonate ($CaCO_3$) precipitation rates would increase A_T but would increase C_T. Even so, the dominant ecosystem in the Bay of Villefranche-sur-Mer is seagrass meadows, which harbor relatively few calcifying organisms. Dissolution of calcium carbonate sediment would contribute to A_T and C_T increase in the water column. However, as the water was supersaturated with respect to both aragonite and calcite, this could only be mediated by biological processes. Carbonate dissolution following CO_2 production via oxic degradation of organic matter releases A_T and C_T in a 1:1 ratio (Moulin et al., 1985).

Likewise, anaerobic remineralization produces alkalinity (Cai et al., 2011). In the sediment of the Bay of Villefranche, sulfate reduction coupled with precipitation of sulfide minerals is the dominant anoxic mineralization pathway (Gaillard et al., 1989). An increase in these processes would explain the observed increase in A_T and C_T, but as trends were slower at 50 m compared to 1 m, this would suggest the dominance of a process taking place in surface waters.

In the upper water column at Point B, changes in biological processes are unlikely to explain the observed trends in A_T and C_T. For example, the concentration of chlorophyll-a, a proxy of primary production, has decreased since 1995, nutrients increased, and phytoplankton blooms have shifted towards earlier dates in the year (Irisson et al., 2012). While a decrease in net primary production could drive C_T trends, the observed increase in NO_3^- and PO_4^{3-} would cause a small decrease in A_T (Wolf-Gladrow et al., 2007). Stimulated community respiration could result from warming waters but enhanced remineralization would cause a decrease in A_T (Wolf-Gladrow et al., 2007).

The lack of salinity change at the surface excludes additional processes as drivers of A_T and C_T increase at Point B. For example, increased summertime evaporation (concentration effect) and reduced freshwater input (decreased dilution effect) would both be expected to cause an increase in salinity, which was not observed. Increased input of Eastern Mediterranean Sea waters could increase A_T, but this is unlikely as this water mass flows much deeper than Point B (Millot and Taupier-Letage, 2005).

Instead, the observed changes in A_T and C_T could be due to increased limestone weathering which would increase the input of A_T from land to the sea via rivers and groundwater. Rivers contribute both A_T and C_T to the Mediterranean Sea (Copin-Montégut, 1993; Tamše et al., 2015). River A_T originates from erosion and is correlated with bedrock composition (e.g., McGrath et al., 2016). Positive trends in river A_T have been documented in

North America and occur via a number of processes including: (1) the interplay of rainfall and land-use (Raymond and Cole, 2003), (2) anthropogenic limestone addition used to enhance agriculture soil pH (Oh and Raymond, 2006; Stets et al., 2014) and freshwater pH (Clair and Hindar, 2005), and (3) potentially indirect effects of anthropogenic CO_2 on groundwater CO_2-acidification and weathering (Macpherson et al., 2008). Such, and other, processes were hypothesized to have driven A_T changes in the Baltic Sea (Müller et al., 2016). There, an increase in A_T of 3.4 μmol kg^{-1} yr^{-1} was observed from 1995 to 2014 (mean salinity = 7). In contrast to Point B, the increase in Baltic Sea A_T was not noticeable at salinity > 30 (Müller et al., 2016).

Given the above speculations, the simplest plausible mechanisms causing the unexpected A_T and C_T trends would be through increasing A_T of the freshwater end-member of Point B. Local precipitation, however, did not have an influential effect and was not correlated with salinity or A_T (Fig. S1). While submarine groundwater springs can be a significant source of nutrients, A_T, and C_T to the ocean (Cai et al., 2003; Slomp and Van Cappellen, 2004), carbonate chemistry contributions of local submarine springs are currently unknown (Gilli, 1995). Signatures of limestone erosion can be observed in A_T of nearby rivers (Var, Paillon, and Roya) but detailed time-series are not available. Likewise, riverine influence at Point B has not been quantified. If river runoff exerts a dominant control on Point B carbonate chemistry, there is a lag effect, as freshwater influence peaked in May but A_T and C_T increased fastest from May through July. Consequently, this hypothesis needs further investigation. Until the source of A_T increase is properly identified, use of this observation in modeling should be implemented with caution.

5. Conclusion

Predictions of coastal ocean acidification remain challenging due the complexity of biogeochemical processes occurring at the ocean-land boundary. At the Point B coastal oceanographic station in the NW Mediterranean Sea, surface ocean acidification was due to atmospheric CO_2 forcing and rapid warming over the observation period 2007-2015. However, additional trends in A_T and C_T were observed and remain unexplained, but these trends could relate to riverine and groundwater input. The influence of coastal boundary processes influencing seawater A_T and C_T presents a potentially major difference between coastal and offshore changes in ocean chemistry. This study highlights the importance of considering other anthropogenic influences in the greater land-sea region that may contribute to coastal biogeochemical cycles (*sensu* Duarte et al. 2013) and alter projections of anthropogenic change in near-shore waters.

Data availability – Time-series data from Point B are available at Pangaea® (doi: 10.1594/PANGAEA.727120)

Author contribution – JPG initiated the study, LM supervised data collection, SA performed SeaFET deployments and calibration, JPG and LK designed and JPG conducted statistical analyses, and LK prepared the manuscript with contributions from all authors.

Competing interests - The authors declare that they have no conflict of interest.

Acknowledgements – Thanks are due to the Service d'Observation Rade de Villefranche (SO-Rade) of the Observatoire Océanologique and the Service d'Observation en Milieu Littoral (SOMLIT/CNRS-INSU) for their kind permission to use the Point B data. Discrete samples were analyzed for C_T and A_T by the *Service National d'Analyse des Paramètres*

Océaniques du CO2. The authors thank Jean-Yves Carval, Anne-Marie Corre, Maïa Durozier, Ornella Passafiume and Frank Petit for sampling assistance, to Steeve Comeau and Alice Webb for help with data analysis, and to Bernard Gentili for producing Fig. 1. Atmospheric CO_2 data from Plateau Rosa was collected by Ricerca sul Sistema Energetico (RSE S.p.A.); we are grateful for their contribution. We acknowledge L. Coppola for providing DYFAMED data (Coppola et al., 2016) and Météo-France for supplying the meteorological data and the HyMeX database teams (ESPRI/IPSL and SEDOO/Observatoire Midi-Pyrenees) for their help in accessing them. The *Agence de l'Eau Rhône-Méditerranée-Corse* kindly provided data on the chemistry of local rivers. Alexandre Dano, Gilles Dandec and Dominique Chassagne provided the high-resolution bathymetric data for the volume estimate of the Bay. We are grateful for helpful comments from Nicolas Metzl on the manuscript and those from two anonymous reviewers. This work is a contribution to the European Project on Ocean Acidification (EPOCA; contract # 211384) and the MedSeA project (contract # 265103), which received funding from the European Community's Seventh Framework Programme, and to the United States National Science Foundation Ocean Sciences Postdoctoral Research Fellowship (OCE-1521597) awarded to LK.

References

Álvarez, M., Sanleón-Bartolomé, H., Tanhua, T., Mintrop, L., Luchetta, A., Cantoni, C., Schroeder, K., and Civitarese, G.: The CO_2 system in the Mediterranean Sea: a basin wide perspective, Ocean Sci., 10, 69-92, 10.5194/os-10-69-2014, 2014.

Aminot, A., and Kérouel, R.: Dosage automatique des nutriments dans les eaux marines: méthodes d'analyse en milieu marin, edited by: Ifremer, 188 pp., 2007.

529 Barbier, E. B., Hacker, S. D., Kennedy, C., Koch, E. W., Stier, A. C., and Silliman, B. R.:
530 The value of estuarine and coastal ecosystem services, Ecol. Monogr., 81, 169-193,
531 10.1890/10-1510.1, 2011.
532 Bates, N. R., Astor, Y. M., Church, M. J., Currie, K., Dore, J. E., González-Dávila, M.,
533 Lorenzoni, L., Muller-Karger, F., Olafsson, J., and Santana-Casiano, J. M.: A time-series
534 view of changing ocean chemistry due to ocean uptake of anthropogenic CO_2 and ocean
535 acidification, Oceanography, 27, 126-141, 2014.
536 Borges, A. V., and Gypens, N.: Carbonate chemistry in the coastal zone responds more
537 strongly to eutrophication than ocean acidification, Limnol. Oceanogr., 55, 346-353,
538 10.4319/lo.2010.55.1.0346, 2010.
539 Bresnahan, P. J., Martz, T. R., Takeshita, Y., Johnson, K. S., and LaShomb, M.: Best
540 practices for autonomous measurement of seawater pH with the Honeywell Durafet,
541 Methods Oceangr., 9, 44-60, 2014.
542 Cai, W.-J., Wang, Y., Krest, J., and Moore, W. S.: The geochemistry of dissolved inorganic
543 carbon in a surficial groundwater aquifer in North Inlet, South Carolina, and the carbon
544 fluxes to the coastal ocean, Geochim. Cosmochim. Acta, 67, 631-639, 10.1016/S0016-
545 7037(02)01167-5, 2003.
546 Cai, W.-J., Hu, X., Huang, W.-J., Murrell, M. C., Lehrter, J. C., Lohrenz, S. E., Chou, W.-C.,
547 Zhai, W., Hollibaugh, J. T., Wang, Y., Zhao, P., Guo, X., Gundersen, K., Dai, M., and
548 Gong, G.-C.: Acidification of subsurface coastal waters enhanced by eutrophication, Nat.
549 Geosci., 4, 766-770, 10.1038/ngeo1297, 2011.
550 Clair, T. A., and Hindar, A.: Liming for the mitigation of acid rain effects in freshwaters: a
551 review of recent results, Environ. Rev., 13, 91-128, 10.1139/a05-009, 2005.
552 Copin-Montégut, C.: Alkalinity and carbon budgets in the Mediterranean Sea, Global
553 Biogeochem. Cycles, 7, 915-925, 10.1029/93GB01826, 1993.

554 Copin-Montégut, C., and Bégovic, M.: Distributions of carbonate properties and oxygen
555 along the water column (0–2000 m) in the central part of the NW Mediterranean Sea
556 (Dyfamed site): influence of winter vertical mixing on air–sea CO_2 and O_2 exchanges,
557 Deep-Sea Res. II, 49, 2049-2066, 10.1016/S0967-0645(02)00027-9, 2002.
558 Coppola, L., Diamond Riquier, E., and Carval, T.: Dyfamed observatory data, SEANOE,
559 10.17882/43749, 2016.
560 Cossarini, G., Lazzari, P., and Solidoro, C.: Spatiotemporal variability of alkalinity in the
561 Mediterranean Sea, Biogeosciences, 12, 1647-1658, 10.5194/bg-12-1647-2015, 2015.
562 Costanza, R., d'Arge, R., de Groot, R., Farber, S., Grasso, M., Hannon, B., Limburg, K.,
563 Naeem, S., O'Neill, R. V., Paruelo, J., Raskin, R. G., Sutton, P., and van den Belt, M.:
564 The value of the world's ecosystem services and natural capital, Nature, 387, 253-260,
565 1997.
566 De Carlo, E. H., Mousseau, L., Passafiume, O., Drupp, P. S., and Gattuso, J.-P.: Carbonate
567 chemistry and air–sea CO_2 flux in a NW Mediterranean bay over a four-year period:
568 2007–2011, Aquatic Geochemistry, 19, 399-442, 10.1007/s10498-013-9217-4, 2013.
569 Dickson, A.: The carbon dioxide system in seawater: equilibrium chemistry and
570 measurements, in: Guide to best practices for ocean acidification research and data
571 reporting, edited by: Fabry, V. J., Hansson, L., and Gattuso, J.-P., Luxembourg:
572 Publications Office of the European Union, 17-40, 2010.
573 Dickson, A. G., and Riley, J. P.: The effect of analytical error on the evaluation of the
574 components of the aquatic carbon-dioxide system, Mar. Chem., 6, 77-85, 10.1016/0304-
575 4203(78)90008-7, 1978.
576 Dickson, A. G.: Standard potential of the reaction: $AgCl(s) + 1/2\ H_2(g) = Ag(s) + HCl(aq)$,
577 and and the standard acidity constant of the ion HSO_4^- in synthetic sea water from 273.15

578 to 318.15 K, The Journal of Chemical Thermodynamics, 22, 113-127, 10.1016/0021-
579 9614(90)90074-Z, 1990.
580 Dickson, A. G., Sabine, C. L., and Christian, J. R.: Guide to best practices for ocean CO_2
581 measurements, PICES Special Publication, 3, 191 pp., 2007.
582 DOE: Handbook of methods for the analysis of the various parameters of the carbon dioxide
583 system in sea water, Carbon Dioxide Information Analysis Center, Oak Ridge National
584 Laboratory, 1994.
585 Doney, S. C., Fabry, V. J., Feely, R. A., and Kleypas, J. A.: Ocean acidification: the other
586 CO_2 problem, Ann. Rev. Mar. Sci., 1, 169-192, 10.1146/annurev.marine.010908.163834,
587 2009.
588 Duarte, C. M., Hendriks, I. E., Moore, T. S., Olsen, Y. S., Steckbauer, A., Ramajo, L.,
589 Carstensen, J., Trotter, J. A., and McCulloch, M.: Is ocean acidification an open-ocean
590 syndrome? Understanding anthropogenic impacts on seawater pH, Estuaries and Coasts,
591 36, 221-236, 10.1007/s12237-013-9594-3, 2013.
592 Edmond, J. M.: High precision determination of titration alkalinity and total carbon dioxide
593 content of sea water by potentiometric titration, Deep-Sea Research, 17, 737-750,
594 10.1016/0011-7471(70)90038-0, 1970.
595 Feely, R. A., Sabine, C. L., Hernandez-Ayon, J. M., Ianson, D., and Hales, B.: Evidence for
596 upwelling of corrosive "acidified" water onto the continental shelf, Science, 320, 1490-
597 1492, 10.1126/science.1155676, 2008.
598 Feely, R. A., Alin, S. R., Newton, J., Sabine, C. L., Warner, M., Devol, A., Krembs, C., and
599 Maloy, C.: The combined effects of ocean acidification, mixing, and respiration on pH
600 and carbonate saturation in an urbanized estuary, Estuar. Coast. Shelf Sci., 88,
601 10.1016/j.ecss.2010.05.004, 2010.

602 Flecha, S., Pérez, F. F., García-Lafuente, J., Sammartino, S., Ríos, A. F., and Huertas, I. E.:
603 Trends of pH decrease in the Mediterranean Sea through high frequency observational
604 data: indication of ocean acidification in the basin, Sci. Rep., 5, 16770,
605 10.1038/srep16770, 2015.
606 Gaillard, J.-F., Pauwels, H., and Michard, G.: Chemical diagenesis in coastal marine
607 sediments, Oceanol. Acta, 12, 175-187, 1989.
608 García-Ibáñez, M. I., Zunino, P., Fröb, F., Carracedo, L. I., Ríos, A. F., Mercier, H., Olsen,
609 A., and Pérez, F. F.: Ocean acidification in the subpolar North Atlantic: rates and
610 mechanisms controlling pH changes, Biogeosciences, 13, 3701-3715, 10.5194/bg-13-
611 3701-2016, 2016.
612 Gattuso, J.-P., Epitalon, J.-M., and Lavigne, H.: seacarb: Seawater Carbonate Chemistry. R
613 package version 3.1.1 https://cran.r-project.org/package=seacarb, 2016.
614 Gattuso, J. P., and Hansson, L.: Ocean acidification, Oxford University Press, Oxford, 2011.
615 Gilli, E.: Etude des sources karstiques sous-marines et littorales des Alpes Maritimes entre
616 Menton et Nice, 41, 1995.
617 Halpern, B. S., Walbridge, S., Selkoe, K. A., Kappel, C. V., Micheli, F., D'Agrosa, C., Bruno,
618 J. F., Casey, K. S., Ebert, C., and Fox, H. E.: A global map of human impact on marine
619 ecosystems, Science, 319, 948-952, 2008.
620 Hofmann, G. E., Smith, J. E., Johnson, K. S., Send, U., Levin, L. A., Micheli, F., Paytan, A.,
621 Price, N. N., Peterson, B., Takeshita, Y., Matson, P. G., Crook, E. D., Kroeker, K. J.,
622 Gambi, M. C., Rivest, E. B., Frieder, C. A., Yu, P. C., and Martz, T. R.: High-frequency
623 dynamics of ocean pH: a multi-ecosystem comparison, PLoS One, 6, e28983,
624 10.1371/journal.pone.0028983, 2011.

625 Howes, E. L., Stemmann, L., Assailly, C., Irisson, J. O., Dima, M., Bijma, J., and Gattuso, J.
626 P.: Pteropod time series from the North Western Mediterranean (1967-2003): impacts of
627 pH and climate variability, Mar. Ecol. Prog. Ser., 531, 193-206, 2015.
628 Ingrosso, G., Giani, M., Comici, C., Kralj, M., Piacentino, S., De Vittor, C., and Del Negro,
629 P.: Drivers of the carbonate system seasonal variations in a Mediterranean gulf, Estuar.
630 Coast. Shelf Sci., 168, 58-70, 10.1016/j.ecss.2015.11.001, 2016.
631 Irisson, J.-O., Webb, A., Passafiume, O., and Mousseau, L.: Detecting hydrologic variations
632 in a long term monitoring time series, Europole Mer Gordon-like conference "Time-series
633 analysis in marine science and application for industry", Brest, France, 17-21 Sept 2012,
634 2012.
635 Jiang, Z.-P., Tyrrell, T., Hydes, D. J., Dai, M., and Hartman, S. E.: Variability of alkalinity
636 and the alkalinity-salinity relationship in the tropical and subtropical surface ocean,
637 Global Biogeochem. Cycles, 28, 729-742, 10.1002/2013GB004678, 2014.
638 Kapsenberg, L., Kelley, A. L., Shaw, E. C., Martz, T. R., and Hofmann, G. E.: Near-shore
639 Antarctic pH variability has implications for biological adaptation to ocean acidification,
640 Sci. Rep., 5, 9638, 10.1038/srep09638, 2015.
641 Kapsenberg, L., and Hofmann, G. E.: Ocean pH time-series and drivers of variability along
642 the northern Channel Islands, California, USA, Limnol. Oceanogr., 61, 953-968,
643 10.1002/lno.10264, 2016.
644 Krasakopoulou, E., Souvermezoglou, E., and Goyet, C.: Anthropogenic CO_2 fluxes in the
645 Otranto Strait (E. Mediterranean) in February 1995, Deep-Sea Res. I, 58, 1103-1114,
646 10.1016/j.dsr.2011.08.008, 2011.
647 Lacoue-Labarthe, T., Nunes, P. A. L. D., Ziveri, P., Cinar, M., Gazeau, F., Hall-Spencer, J.
648 M., Hilmi, N., Moschella, P., Safa, A., Sauzade, D., and Turley, C.: Impacts of ocean

649 acidification in a warming Mediterranean Sea: An overview, Regional Studies in Marine
650 Science, 5, 1-11, 10.1016/j.rsma.2015.12.005, 2016.
651 Le Quéré, C., Andrew, R. M., Canadell, J. G., Sitch, S., Korsbakken, J. I., Peters, G. P.,
652 Manning, A. C., Boden, T. A., Tans, P. P., Houghton, R. A., Keeling, R. F., Alin, S.,
653 Andrews, O. D., Anthoni, P., Barbero, L., Bopp, L., Chevallier, F., Chini, L. P., Ciais, P.,
654 Currie, K., Delire, C., Doney, S. C., Friedlingstein, P., Gkritzalis, T., Harris, I., Hauck, J.,
655 Haverd, V., Hoppema, M., Klein Goldewijk, K., Jain, A. K., Kato, E., Körtzinger, A.,
656 Landschützer, P., Lefèvre, N., Lenton, A., Lienert, S., Lombardozzi, D., Melton, J. R.,
657 Metzl, N., Millero, F., Monteiro, P. M. S., Munro, D. R., Nabel, J. E. M. S., Nakaoka, S.
658 I., O'Brien, K., Olsen, A., Omar, A. M., Ono, T., Pierrot, D., Poulter, B., Rödenbeck, C.,
659 Salisbury, J., Schuster, U., Schwinger, J., Séférian, R., Skjelvan, I., Stocker, B. D.,
660 Sutton, A. J., Takahashi, T., Tian, H., Tilbrook, B., van der Laan-Luijkx, I. T., van der
661 Werf, G. R., Viovy, N., Walker, A. P., Wiltshire, A. J., and Zaehle, S.: Global Carbon
662 Budget 2016, Earth Syst. Sci. Data, 8, 605-649, 10.5194/essd-8-605-2016, 2016.
663 Lee, K., Kim, T.-W., Byrne, R. H., Millero, F. J., Feely, R. A., and Liu, Y.-M.: The universal
664 ratio of boron to chlorinity for the North Pacific and North Atlantic oceans, Geochim.
665 Cosmochim. Acta, 74, 1801-1811, 10.1016/j.gca.2009.12.027, 2010.
666 Lee, K., Sabine, C. L., Tanhua, T., Kim, T.-W., Feely, R. A., and Kim, H.-C.: Roles of
667 marginal seas in absorbing and storing fossil fuel CO_2, Energy & Environmental Science,
668 4, 1133-1146, 10.1039/C0EE00663G, 2011.
669 Lejeusne, C., Chevaldonné, P., Pergent-Martini, C., Boudouresque, C. F., and Pérez, T.:
670 Climate change effects on a miniature ocean: the highly diverse, highly impacted
671 Mediterranean Sea, Trends Ecol. Evol., 25, 250-260,
672 http://dx.doi.org/10.1016/j.tree.2009.10.009, 2010.

673 Luchetta, A., Cantoni, C., and Catalano, G.: New observations of CO_2-induced acidification
674 in the northern Adriatic Sea over the last quarter century, Chem. Ecol., 26, 1-17,
675 10.1080/02757541003627688, 2010.
676 Lueker, T. J., Dickson, A. G., and Keeling, C. D.: Ocean pCO_2 calculated from dissolved
677 inorganic carbon, alkalinity, and equations for K_1 and K_2: validation based on laboratory
678 measurements of CO_2 in gas and seawater at equilibrium, Mar. Chem., 70, 105-119,
679 10.1016/S0304-4203(00)00022-0, 2000.
680 Macpherson, G. L., Roberts, J. A., Blair, J. M., Townsend, M. A., Fowle, D. A., and Beisner,
681 K. R.: Increasing shallow groundwater CO_2 and limestone weathering, Konza Prairie,
682 USA, Geochim. Cosmochim. Acta, 72, 5581-5599, 10.1016/j.gca.2008.09.004, 2008.
683 Marcellin Yao, K., Marcou, O., Goyet, C., Guglielmi, V., Touratier, F., and Savy, J.-P.: Time
684 variability of the north-western Mediterranean Sea pH over 1995–2011, Mar. Environ.
685 Res., 116, 51-60, 10.1016/j.marenvres.2016.02.016, 2016.
686 McGrath, T., McGovern, E., Cave, R. R., and Kivimäe, C.: The inorganic carbon chemistry
687 in coastal and shelf waters around Ireland, Estuaries and Coasts, 39, 27-39,
688 10.1007/s12237-015-9950-6, 2016.
689 Meier, K. J. S., Beaufort, L., Heussner, S., and Ziveri, P.: The role of ocean acidification in
690 *Emiliania huxleyi* coccolith thinning in the Mediterranean Sea, Biogeosciences, 11, 2857-
691 2869, 10.5194/bg-11-2857-2014, 2014.
692 The MerMex Group, Durrieu de Madron, X., Guieu, C., Sempéré, R., Conan, P., Cossa, D.,
693 D'Ortenzio, F., Estournel, C., Gazeau, F., Rabouille, C., Stemmann, L., Bonnet, S., Diaz,
694 F., Koubbi, P., Radakovitch, O., Babin, M., Baklouti, M., Bancon-Montigny, C., Belviso,
695 S., Bensoussan, N., Bonsang, B., Bouloubassi, I., Brunet, C., Cadiou, J. F., Carlotti, F.,
696 Chami, M., Charmasson, S., Charrière, B., Dachs, J., Doxaran, D., Dutay, J. C., Elbaz-
697 Poulichet, F., Eléaume, M., Eyrolles, F., Fernandez, C., Fowler, S., Francour, P.,

698 Gaertner, J. C., Galzin, R., Gasparini, S., Ghiglione, J. F., Gonzalez, J. L., Goyet, C.,
699 Guidi, L., Guizien, K., Heimbürger, L. E., Jacquet, S. H. M., Jeffrey, W. H., Joux, F., Le
700 Hir, P., Leblanc, K., Lefèvre, D., Lejeusne, C., Lemé, R., Loÿe-Pilot, M. D., Mallet, M.,
701 Méjanelle, L., Mélin, F., Mellon, C., Mérigot, B., Merle, P. L., Migon, C., Miller, W. L.,
702 Mortier, L., Mostajir, B., Mousseau, L., Moutin, T., Para, J., Pérez, T., Petrenko, A.,
703 Poggiale, J. C., Prieur, L., Pujo-Pay, M., Pulido, V., Raimbault, P., Rees, A. P., Ridame,
704 C., Rontani, J. F., Ruiz Pino, D., Sicre, M. A., Taillandier, V., Tamburini, C., Tanaka, T.,
705 Taupier-Letage, I., Tedetti, M., Testor, P., Thébault, H., Thouvenin, B., Touratier, F.,
706 Tronczynski, J., Ulses, C., Van Wambeke, F., Vantrepotte, V., Vaz, S., and Verney, R.:
707 Marine ecosystems' responses to climatic and anthropogenic forcings in the
708 Mediterranean, Prog. Oceanogr., 91, 97-166, 10.1016/j.pocean.2011.02.003, 2011.
709 Millot, C., and Taupier-Letage, I.: Circulation in the Mediterranean Sea, in: The
710 Mediterranean Sea, edited by: Saliot, A., Springer Berlin Heidelberg, Berlin, Heidelberg,
711 29-66, 2005.
712 Moulin, E., Jordens, A., and Wollast, R.: Influence of the aerobic bacterial respiration on the
713 early dissolution of carbonates in coastal sediments, in: Progress in Belgian
714 Oceanographic Research: Proceedings of a Symposium Held at the Palace of Academies
715 Brussels, edited by: Van Grieken, R., and Wollast, R., Brussels, 196-208, 1985.
716 Müller, J. D., Schneider, B., and Rehder, G.: Long-term alkalinity trends in the Baltic Sea
717 and their implications for CO_2-induced acidification, Limnol. Oceanogr.,
718 10.1002/lno.10349, 2016.
719 Oh, N.-H., and Raymond, P. A.: Contribution of agricultural liming to riverine bicarbonate
720 export and CO_2 sequestration in the Ohio River basin, Global Biogeochem. Cycles, 20,
721 GB3012, 10.1029/2005GB002565, 2006.

722 Omstedt, A., Edman, M., Claremar, B., and Rutgersson, A.: Modelling the contributions to
723 marine acidification from deposited SO_x, NO_x, and NH_x in the Baltic Sea: Past and
724 present situations, Cont. Shelf Res., 111, Part B, 234-249, 10.1016/j.csr.2015.08.024,
725 2015.
726 Palmiéri, J., Orr, J., Dutay, J., Béranger, K., Schneider, A., Beuvier, J., and Somot, S.:
727 Simulated anthropogenic CO_2 storage and acidification of the Mediterranean Sea,
728 Biogeosciences, 12, 781-802, 2015.
729 Parravicini, V., Mangialajo, L., Mousseau, L., Peirano, A., Morri, C., Montefalcone, M.,
730 Francour, P., Kulbicki, M., and Bianchi, C. N.: Climate change and warm-water species
731 at the north-western boundary of the Mediterranean Sea, Mar. Ecol., 36, 897-909,
732 10.1111/maec.12277, 2015.
733 Perez, F. F., and Fraga, F.: The pH measurements in seawater on the NBS scale, Mar. Chem.,
734 21, 315-327, 10.1016/0304-4203(87)90054-5, 1987.
735 Pörtner, H.-O., Karl, D., Boyd, P. W., Cheung, W., Lluch-Cota, S. E., Nojiri, Y., Schmidt, D.
736 N., and Zavialov, P.: Ocean systems, in: Climate Change 2014: Impacts, Adaptation, and
737 Vulnerability. Part A: Global and Sectoral Aspects. Contribution of Working Group II to
738 the Fifth Assessment Report of the Intergovernmental Panel on Climate Change, edited
739 by: Field, C. B., Barros, V. R., Dokken, D. J., Mach, K. J., Mastrandrea, M. D., Bilir, T.
740 E., Chatterjee, M., Ebi, K. L., Estrada, Y. O., Genova, R. C., Girma, B., Kissel, E. S.,
741 Levy, A. N., MacCracken, S., Mastrandrea, P. R., and L.L.White, Cambridge University
742 Press, Cambridge, United Kingdom and New York, NY, USA, 411-484, 2014.
743 Provoost, P., van Heuven, S., Soetaert, K., Laane, R. W. P. M., and Middelburg, J. J.:
744 Seasonal and long-term changes in pH in the Dutch coastal zone, Biogeosciences, 7,
745 3869-3878, 10.5194/bg-7-3869-2010, 2010.

746 Raymond, P. A., and Cole, J. J.: Increase in the export of alkalinity from North America's
747 largest river, Science, 301, 88-91, 2003.
748 Rhein, M., Rintoul, S. R., Aoki, S., Campos, E., Chambers, D., Feely, R. A., Gulev, S.,
749 Johnson, G. C., Josey, S. A., A. Kostianoy, Mauritzen, C., Roemmich, D., Talley, L. D.,
750 and Wang, F.: Observations: Ocean, in: Climate Change 2013: The Physical Science
751 Basis. Contribution of Working Group I to the Fifth Assessment Report of the
752 Intergovernmental Panel on Climate Change, edited by: Stocker, T. F., Qin, D., Plattner,
753 G.-K., Tignor, M., Allen, S. K., Boschung, J., Nauels, A., Xia, Y., Bex, V., and Midgley,
754 P. M., Cambridge University Press, Cambridge, United Kingdom and New York, NY,
755 USA., 2013.
756 Schneider, A., Wallace, D. W. R., and Körtzinger, A.: Alkalinity of the Mediterranean Sea,
757 Geophys. Res. Lett., 34, L15608, 10.1029/2006GL028842, 2007.
758 Schneider, A., Tanhua, T., Körtzinger, A., and Wallace, D. W. R.: High anthropogenic
759 carbon content in the eastern Mediterranean, J. Geophys. Res., 115, C12050,
760 10.1029/2010JC006171, 2010.
761 Slomp, C. P., and Van Cappellen, P.: Nutrient inputs to the coastal ocean through submarine
762 groundwater discharge: controls and potential impact, Journal of Hydrology, 295, 64-86,
763 10.1016/j.jhydrol.2004.02.018, 2004.
764 Stets, E. G., Kelly, V. J., and Crawford, C. G.: Long-term trends in alkalinity in large rivers
765 of the conterminous US in relation to acidification, agriculture, and hydrologic
766 modification, Sci. Total Environ., 488–489, 280-289, 10.1016/j.scitotenv.2014.04.054,
767 2014.
768 Tamše, S., Ogrinc, N., Walter, L. M., Turk, D., and Faganeli, J.: River sources of dissolved
769 inorganic carbon in the Gulf of Trieste (N Adriatic): stable carbon isotope evidence,
770 Estuaries and Coasts, 38, 151-164, 10.1007/s12237-014-9812-7, 2015.

771 Tanhua, T., Bates, N. R., and Körtzinger, A.: The marine carbon cycle and ocean
772 anthropogenic CO_2 inventories, in: Ocean Circulation and Climate: A 21st Century
773 Perspective. 2nd Ed, edited by: Siedler, G., Griffies, S., Gould, J., and Church, J., 103,
774 Academic Press, 787-816, 2013.
775 Team, R. C.: R: A language and environment for statistical computing. R Foundation for
776 Statistical Computing, Vienna, Austria. https://www.r-project.org/, 2016.
777 Touratier, F., and Goyet, C.: Impact of the Eastern Mediterranean Transient on the
778 distribution of anthropogenic CO_2 and first estimate of acidification for the Mediterranean
779 Sea, Deep-Sea Res. I, 58, 1-15, 10.1016/j.dsr.2010.10.002, 2011.
780 Touratier, F., Goyet, C., Houpert, L., de Madron, X. D., Lefèvre, D., Stabholz, M., and
781 Guglielmi, V.: Role of deep convection on anthropogenic CO_2 sequestration in the Gulf
782 of Lions (northwestern Mediterranean Sea), Deep-Sea Res. I, 113, 33-48,
783 10.1016/j.dsr.2016.04.003, 2016.
784 Vargas, C. A., Contreras, P. Y., Pérez, C. A., Sobarzo, M., Saldías, G. S., and Salisbury, J.:
785 Influences of riverine and upwelling waters on the coastal carbonate system off Central
786 Chile and their ocean acidification implications, Journal of Geophysical Research:
787 Biogeosciences, 121, 1468-1483, 10.1002/2015JG003213, 2016.
788 Wolf-Gladrow, D. A., Zeebe, R. E., Klaas, C., Körtzinger, A., and Dickson, A. G.: Total
789 alkalinity: The explicit conservative expression and its application to biogeochemical
790 processes, Mar. Chem., 106, 287-300, 10.1016/j.marchem.2007.01.006, 2007.
791 Wootton, J. T., Pfister, C. A., and Forester, J. D.: Dynamic patterns and ecological impacts of
792 declining ocean pH in a high-resolution multi-year dataset, Proc. Natl. Acad. Sci., 105,
793 18848-18853, 2008.
794 Wootton, J. T., and Pfister, C. A.: Carbon system measurements and potential climatic
795 drivers at a site of rapidly declining ocean pH, PLoS One, 7, e53396, 2012.

796 **Table 1.** Previous estimates or documentation of pH change (ΔpH**)** in the Mediterranean Sea.
797 'Total' indicates estimates made for the whole Mediterranean Sea. TrOCA is the 'Tracer
798 combining Oxygen, inorganic Carbon, and total Alkalinity' method, NR means 'not
799 reported', and PI is 'pre-industrial era'. *indicates studies where the reported pH change was
800 assumed to be at *in situ* temperatures.

Region	***Site***	***Method***	***Study period***	***pH scale***	***°C***	***ΔpH yr^{-1} ± SE***	***Total ΔpH***	***Reference***
NW	Point B, 1 m	time-series, anomaly	2007-2015	total	*in situ*	-0.0028 ± 0.0003	-0.0252	This study
NW	Point B, 1 m	time-series, anomaly	2007-2015	total	25	-0.0017 ± 0.0002	-0.0153	This study
NW	Point B	model	1967-2003	total	*in situ*	-0.0014	-0.05	Howes et al. (2015)
NW	DYFAMED	time-series, observed	1995-2011	seawater	*in situ*	-0.003 ± 0.001	-0.051	Marcellin Yao et al. (2016
NW	DYFAMED	time-series comparison	1998-2000, 2003-2005	seawater	*in situ**	-	-0.02	Meier et al. (2014)
NW	Gulf of Lion	TrOCA	PI-2011	NR	*in situ**	-	-0.15 to -0.11	Touratier et al. (2016)
East	N Adriatic Sea	cruise comparison	1983, 2008	total	25	-0.0025	-0.063	Luchetta et al. (2010)
East	Otranto Strait	TrOCA	PI-1995	seawater	25	-	< -0.1 to -0.05, ± 0.014	Krasakopoulou et al. (2011)
Total	Full profile	TrOCA	PI-2001	NR	*in situ**	-	-0.14 to -0.05	Touratier and Goyet (2011
Total	Bottom waters	model	1800-2001	total	*in situ**	-	-0.06 to -0.005	Palmiéri et al. (2015)
Total	Surface waters	model	1800-2001	total	*in situ**	-	-0.084 ± 0.001	Palmiéri et al. (2015)
Gibraltar Strait	Espartel sill	pH, pCO_2 sensors	2012-2015	total	25	-0.0044 ± 0.00006	-	Flecha et al. (2015)

801

802

803 **Table 2.** Time-series anomaly regression analyses on seawater carbonate chemistry at Point
804 B for salinity (S), temperature (T), dissolved inorganic carbon (C_T), total alkalinity (A_T), pH_T,
805 pH_T normalized to 25 ºC (pH_{T25}), pCO_2, calcite (Ω_c) and aragonite (Ω_a) saturation state, and
806 salinity-normalized A_T (nA_T) and C_T (nC_T), at 1 and 50 m. Slopes represent the change in the
807 variable unit per year. P <<0.001 indicates p-values far smaller than 0.001.

Depth (m)	*Variable*	*Slope ± SE*	*Intercept ± SE*	*N*	*F*	*df*	*Slope P*	R^2
1	S	-0.0017 ± 0.0044	3.38 ± 8.82	417	0.147	1,415	0.702	0
	T (ºC)	0.072 ± 0.022	-145 ± 44	413	10.999	1,411	0.001	0.026
	C_T (µmol kg^{-1})	2.97 ± 0.20	-5965 ± 400	416	221.87	1,414	<<0.001	0.349
	A_T (µmol kg^{-1})	2.08 ± 0.19	-4189 ± 379	417	122.429	1,415	<<0.001	0.228
	pH_T	-0.0028 ± 0.0003	5.72 ± 0.66	412	74.205	1,410	<<0.001	0.153
	pH_{T25}	-0.0017 ± 0.0002	3.46 ± 0.43	412	64.204	1, 410	<<0.001	0.1354
	pCO_2 (µatm)	3.53 ± 0.39	-7105 ± 776	412	83.927	1,410	<<0.001	0.17
	Ω_c	-0.0109 ± 0.0022	22.0 ± 4.5	412	24.08	1,410	<<0.001	0.055
	Ω_a	-0.0064 ± 0.0015	12.9 ± 3.1	412	17.33	1,410	<<0.001	0.041
	nA_T (µmol kg^{-1})	2.20 ± 0.28	-4425 ± 560	412	62.34	1,410	<<0.001	0.132
	nC_T (µmol kg^{-1})	3.12 ± 0.29	-6275 ± 579	412	117.486	1,410	<<0.001	0.223
50	S	0.0063 ± 0.0020	-12.8 ± 4.1	412	9.858	1, 410	0.002	0.0235
	T (ºC)	0.088 ± 0.019	-177 ± 38	408	21.927	1, 406	<<0.001	0.0512
	C_T (µmol kg^{-1})	2.16 ± 0.21	-4344 ± 418	411	108.105	1, 409	<<0.001	0.2091
	A_T (µmol kg^{-1})	1.59 ± 0.15	-3192 ± 309	412	106.947	1, 410	<<0.001	0.2069
	pH_T	-0.0026 ± 0.0002	5.28 ± 0.50	407	112.111	1, 405	<<0.001	0.2168
	pH_{T25}	-0.0013 ± 0.0003	2.55 ± 0.54	407	21.863	1, 405	<<0.001	0.0512
	pCO_2 (µatm)	2.79 ± 0.25	-5603 ± 501	407	125.1	1, 405	<<0.001	0.236
	Ω_c	-0.0070 ± 0.0027	14.0 ± 5.4	407	6.648	1, 405	0.01	0.0162
	Ω_a	-0.0038 ± 0.0019	7.6 ± 3.7	407	4.155	1, 405	0.042	0.0102
	nA_T (µmol kg^{-1})	1.15 ± 0.13	-2309 ± 254	407	82.309	1, 405	<<0.001	0.1689
	nC_T (µmol kg^{-1})	1.82 ± 0.19	-3661 ± 376	407	94.98	1, 405	<<0.001	0.19

808

809

Table 3. Deconvolution of pH_T anomalies ($\frac{dpH_T}{dt}$, units pH_T yr^{-1}) at 1 and 50 m. Sensitivity of pH_T with respect to variables ($\frac{\partial pH_T}{\partial var}$), where the variable *var* is either temperature (T), salinity (S), total alkalinity (A_T), or dissolved inorganic carbon (C_T), was multiplied by the anomaly of *var* ($\frac{dvar}{dt}$, Table 2). SE is standard error and RMSE is root-mean-squared error. Rounding was performed at the end of the calculations, prior to estimating percent contributions.

Depth (m)	***var***	$\frac{\partial pH_T}{\partial var} \pm SE$	$\frac{\partial pH_T}{\partial var}\frac{dvar}{dt} \pm RMSE$	***Contribution (%)***	$\frac{dpH_T}{dt} \pm RMSE$
1	T (ºC)	-0.0153 ± <0.0001	-0.0011 ± 0.0003	41	-0.0027 ± 0.0005
	S	-0.0117 ± <0.0001	<0.0001 ± 0.0001	0	
	A_T (µmol kg^{-1})	0.0015 ± <0.0001	0.0031 ± 0.0003	-115	
	C_T (µmol kg^{-1})	-0.0016 ± <0.0001	-0.0047 ± 0.0003	174	
50	T (ºC)	-0.0154 ± <0.0001	-0.0014 ± 0.0003	54	-0.0026 ± 0.0005
	S	-0.0116 ± <0.0001	-0.0001 ± <0.0001	4	
	A_T (µmol kg^{-1})	0.0015 ± <0.0001	0.0024 ± 0.0002	-92	
	C_T (µmol kg^{-1})	-0.0016 ± <0.0001	-0.0035 ± 0.0003	135	

817 **Table 4.** Deconvolution of pCO_2 anomalies ($\frac{dpCO_2}{dt}$, µatm yr^{-1}) at 1 and 50 m. Details are the

818 same as in Table 3.

Depth (m)	***var***	$\frac{\partial pCO_2}{\partial var} \pm SE$	$\frac{\partial pCO_2}{\partial var}\frac{dvar}{dt} \pm RMSE$	***Contribution (%)***	$\frac{dpCO_2}{dt} \pm RMSE$
1	T (ºC)	16.49 ± 0.05	1.19 ± 0.36	37	3.23 ± 0.57
	S	10.14 ± <0.01	-0.02 ± 0.05	-1	
	A_T (µmol kg^{-1})	-1.478 ± 0.005	-3.08 ± 0.28	-95	
	C_T (µmol kg^{-1})	1.735 ± 0.006	5.14 ± 0.35	159	
50	T (ºC)	15.55 ± 0.03	1.37 ± 0.29	48	2.84 ± 0.49
	S	9.355 ± <0.001	0.06 ± 0.02	2	
	A_T (µmol kg^{-1})	-1.327 ± 0.002	-2.11 ± 0.20	-74	
	C_T (µmol kg^{-1})	1.629 ± 0.005	3.52 ± 0.34	124	

819

820 **Figure 1.** Map of study region in the NW Mediterranean Sea (a), along the North current (b)
821 in the Bay of Villefranche-sur-Mer, France (c). Point B, EOL buoy, and the offshore time-
822 series station DYFAMED are marked. Bathymetric line units are m (c).

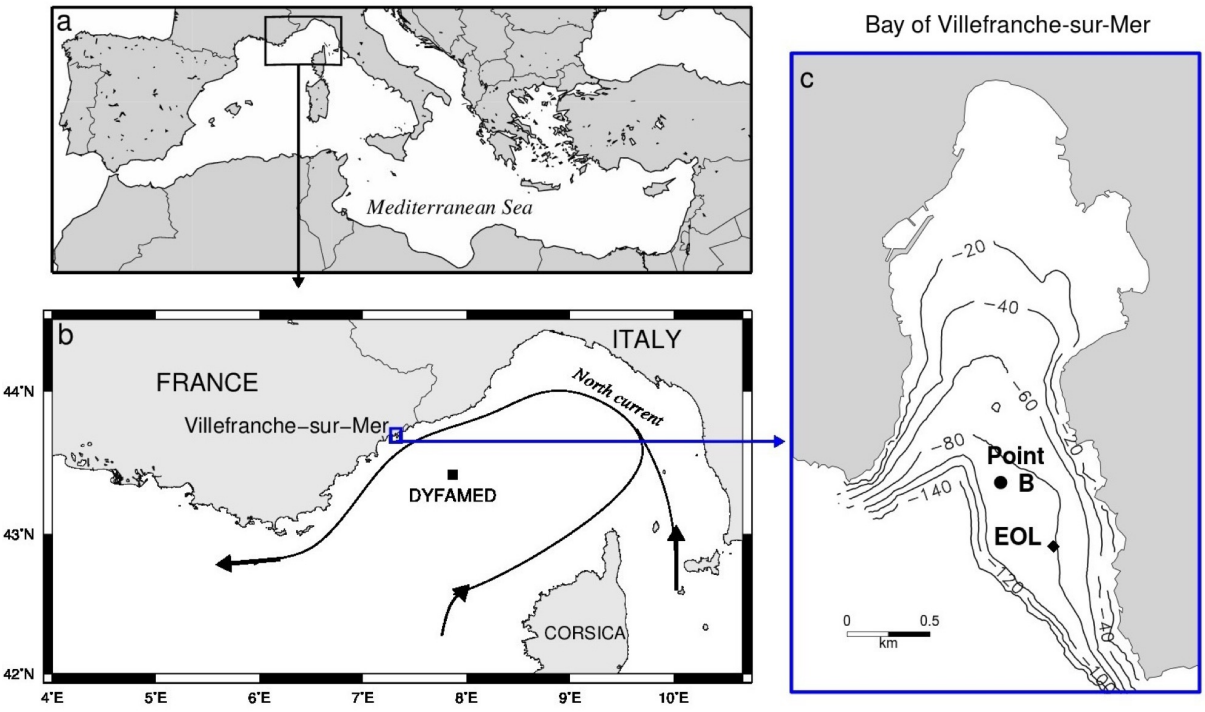

823

Figure 2. Time-series observations (a-g) and anomaly trends (h-n) for temperature, salinity, and seawater carbonate chemistry at Point B, 1 m. Regression slopes are drawn ± SE (in grey) and noted with a star for significance at $\alpha = 0.05$. Variable abbrevations are the same as in Table 2.

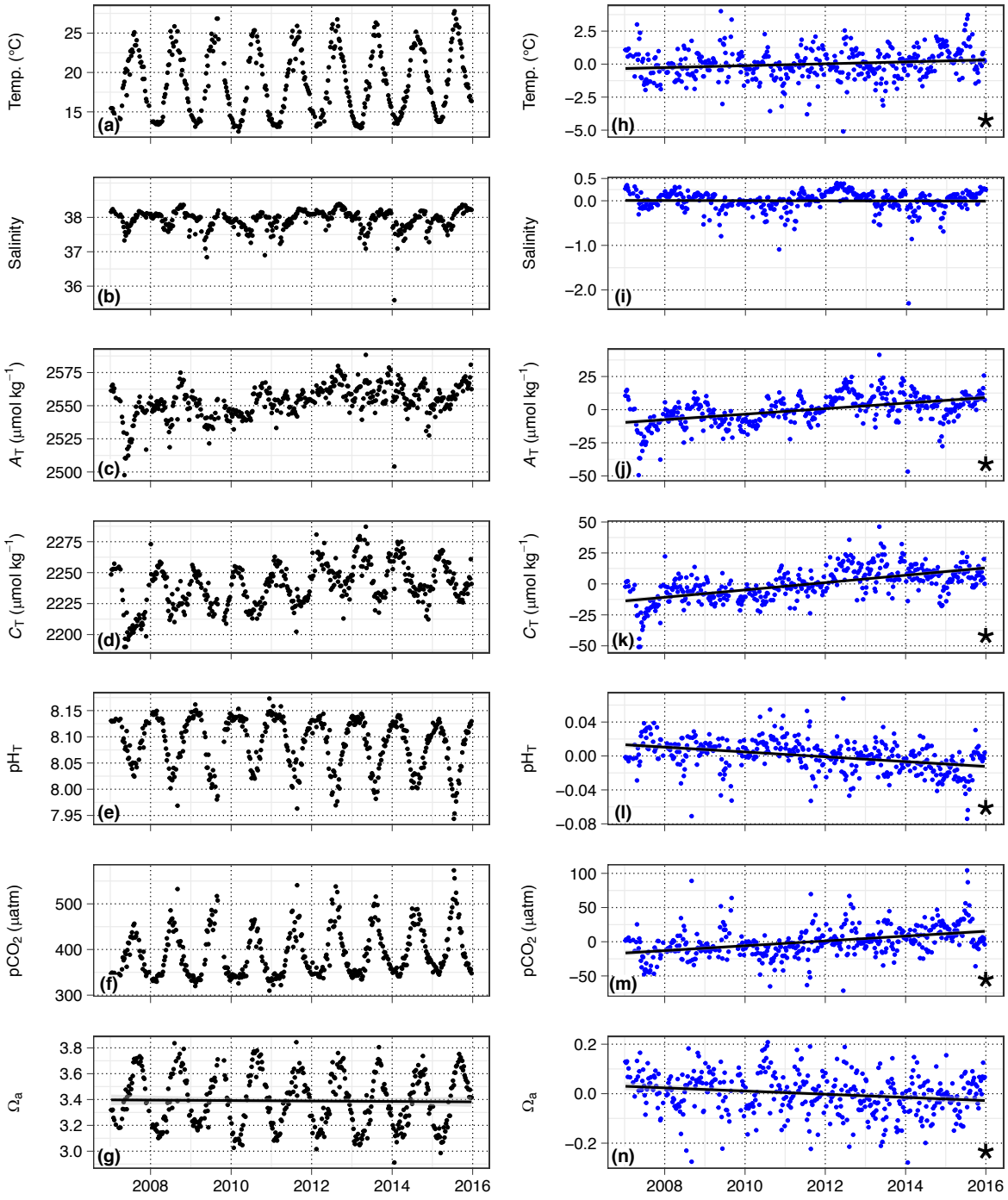

Figure 3. Time-series observations (a-g) and anomaly trends (h-n) for temperature, salinity, and seawater carbonate chemistry at Point B, 50 m. Regression slopes are drawn ± SE (in grey) and noted with a star for significance at $\alpha = 0.05$. Variable abbrevations are the same as in Table 2.

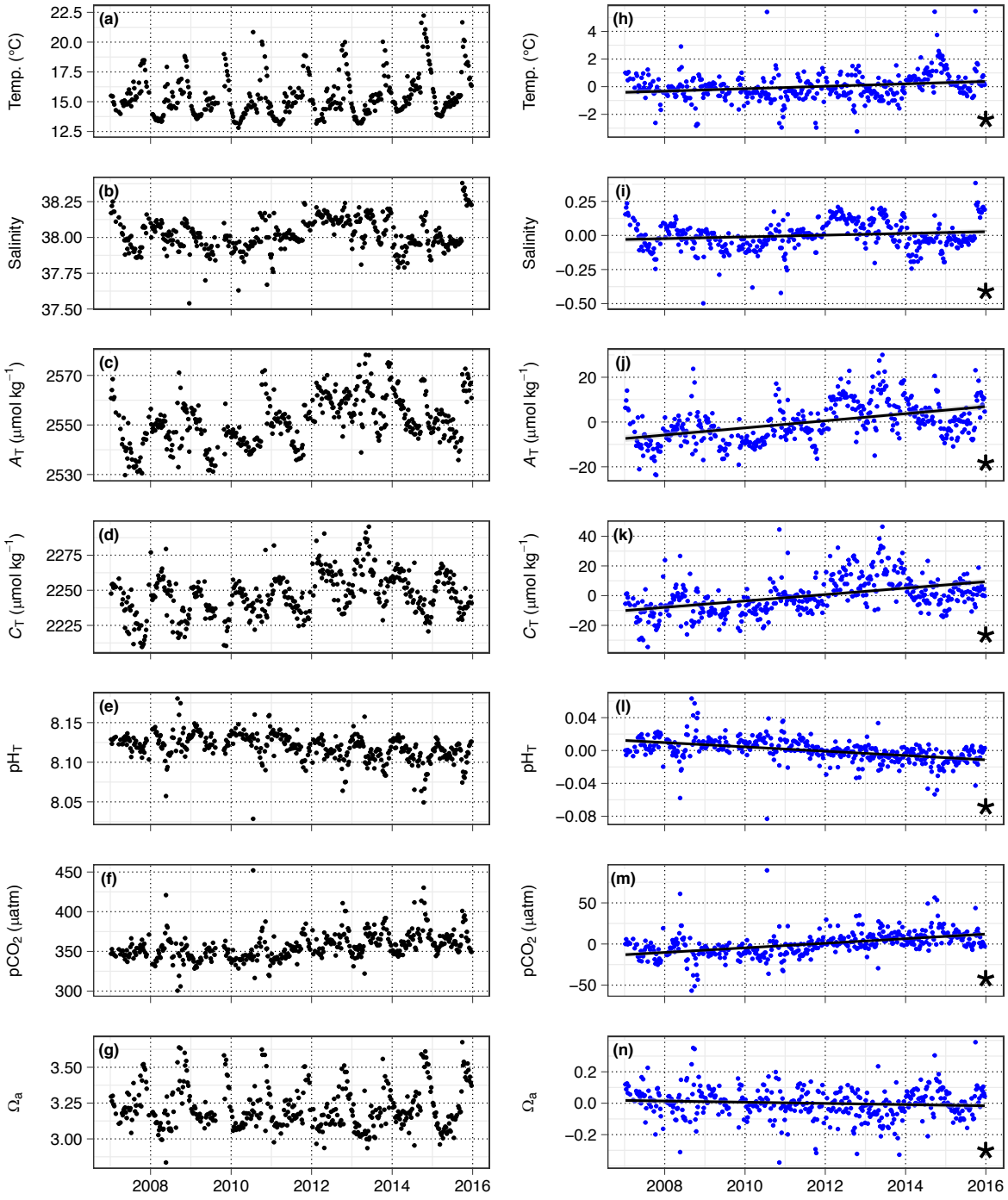

Figure 4. Monthly distribution of seawater carbonate chemistry at Point B, 1 m, using a combination of a violin plot showing the relative frequency of the observations (shaded blue area) and a boxplot showing the median, first and third quartiles, as well as outliers (blue).

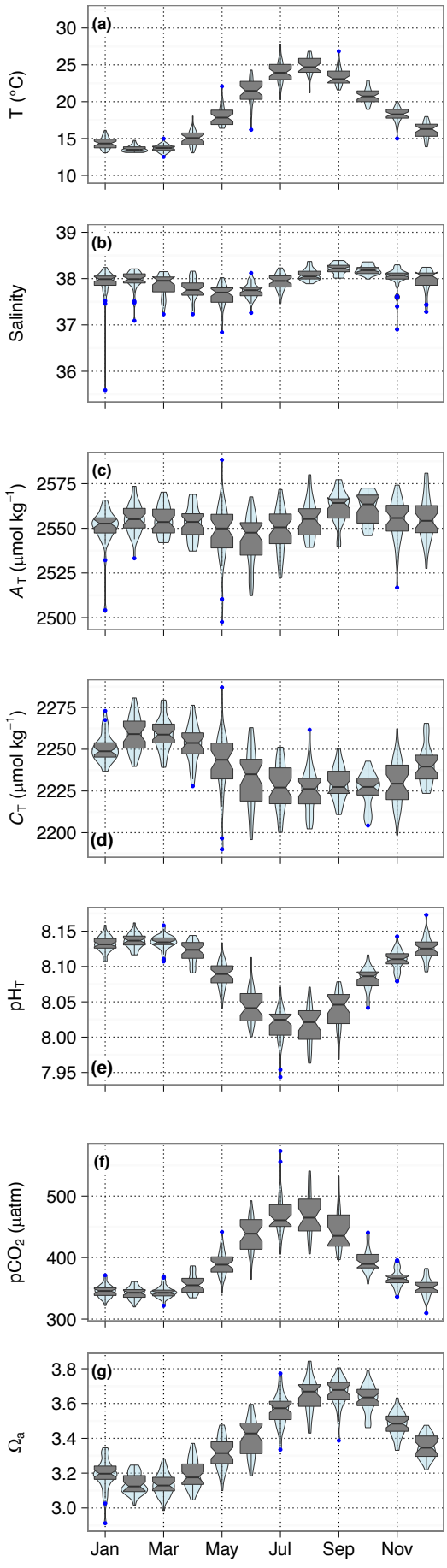

841 **Figure 5.** Monthly trends of total alkalinity (A_T, blue) and dissolved inorganic carbon (C_T,

842 green) for the period 2007-2015. Errors bars are ± SE of the slope estimate and significance

843 is noted (*) at $\alpha = 0.05$.

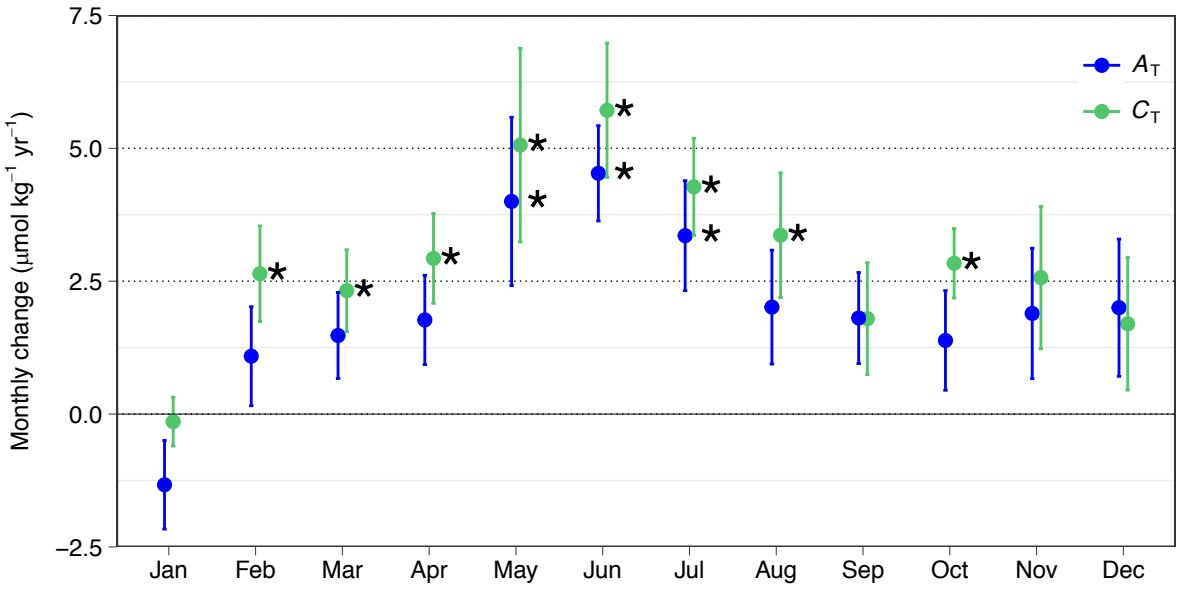

844

Figure 6. Salinity and total alkalinity (A_T) relationships at Point B for the period 2007-2015, by year, at 1 m. Data points are colored for month.

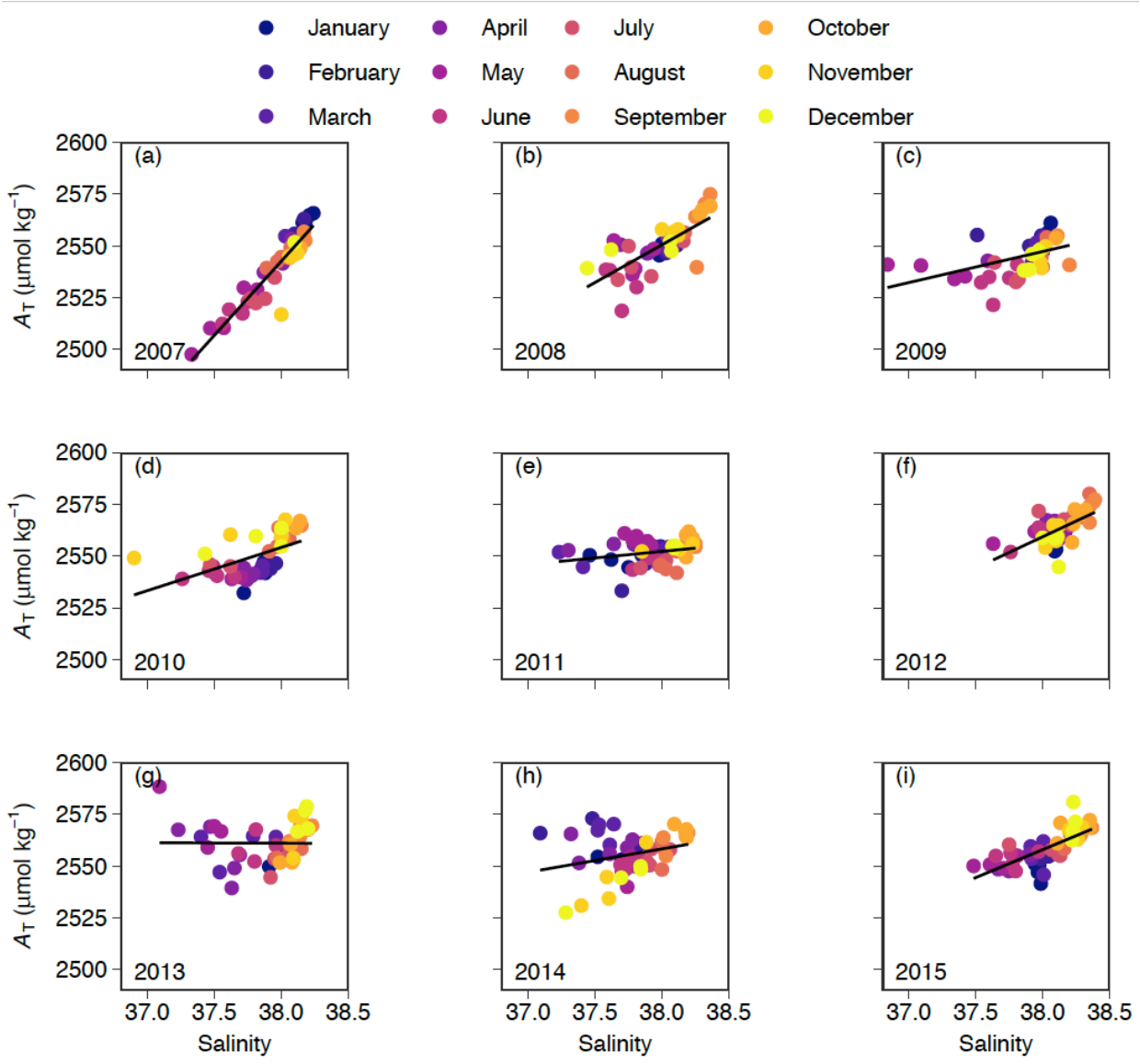

Figure 7. Time-series pH_T (a) and temperature (b) from SeaFET pH sensor deployments at EOL, 2 m. Discrete calibration samples are noted in green, and grey vertical lines bracket deployment periods (a). Calibration sample offsets from processed pH time-series are shown in panel (c). Violin and boxplots (see Fig. 4) show diel pH range by month (d), and an example of this pH variability is shown for May 2015 (e).